EGUSPHERE-2025-5668 | Research article

Seasonal and interannual variability of atmospheric ammonia over Guatemala driven by land use, biomass burning, and meteorological circulation

Christian Saravia et al. (2025)

Response to Reviewer 2

We sincerely thank the reviewer for their time, and constructive feedback on our manuscript. We have carefully addressed all suggestions and implemented the corresponding changes, which have substantially identified areas for improvement of the manuscript. We acknowledge the identification of several important conceptual, structural, and issues that require substantial revision. The reviewer's comments are listed in **black**, followed by our response in "blue", with updated manuscript in "*blue*".

General comments:

This paper presents the first study on the seasonal and interannual trends of NH3 over Guatemala using IASI A, B, and C total columns. By combining satellite observations with land use and fire data, the authors conclude that the NH3 trends over Guatemala between 2015 and 2023 were mainly driven by agricultural emissions and episodic fire events.

A number of studies have used IASI observations to look at NH3 trends and variabilities at country and regional scales, but most focused on major agricultural regions such as North America, Europe, and Asia, where elevated NH3 plumes are easily detectable from space because the column concentrations are one to two orders of magnitude higher than the instrument's detection limit. This study adds value to the existing body of literature because NH3 concentrations in Guatemala are generally near the detection limit of IASI, shedding light on the technical limitations of satellite measurements. This is a potentially interesting point that remains under-explored in the current paper.

The paper also needs some reorganization. For example, in the first paragraph of Methodology, the authors are already discussing results. This section should start with a description of the datasets and mathematical/statistical methods used, which are currently placed later in the section. My other concerns and questions can be found below.

Major comments:

L41-49: This paragraph heavily focuses on vehicle emissions as an underestimated source of NH3, so I was expecting to see some analysis on vehicle emissions, but there were none except one sentence mentioning that traffic activity decreased in April 2020. If you are not going to delve into traffic emissions, I recommend shortening this paragraph to one sentence just saying

that vehicle emissions remain an underestimated source in NH3 emission inventories and merging it with the previous paragraph.

We agree that the previous paragraph mentioned vehicle emissions without providing any analysis. In the revised manuscript, we have shortened and merge with the previous paragraph. Vehicles emission now mentioned only briefly as underestimated no agricultural source.

REVISED MANUSCRIPT (L31-L39)

NH_3 is also a key component in atmospheric chemistry and in the coupling of nitrogen and carbon cycles within ecosystems, with broad consequences regarding climate regulation, agricultural sustainability, air quality and public health. NH_3 emissions originate from both natural and anthropogenic activities, with the latter contributing the majority of the global NH_3 burden. The agricultural sector remains the principal source, accounting for over 81% of total anthropogenic emissions globally (Van Damme et al., 2021; Wyer et al., 2022), while additional anthropogenic contributions stem from residential combustion, vehicular exhaust, industrial production, and wastewater treatment systems (Abeed et al., 2022; Dragosits et al., 2002; Sutton et al., 2007). Although agriculture particularly using fertilizers and manure remains the dominant source of atmospheric NH_3. Nonagricultural sources such as vehicular and industrial emission may be also contribute and are significantly underestimated (Chen et al., 2024; Chen and Wang, 2025; Farren et al., 2020; Gu et al., 2023; Zhou et al., 2017). ~~Empirical evidence indicates that diesel vehicles equipped with selective catalytic reduction (SCR) systems can emit NH_3 as an unintended byproduct (Sun et al., 2017; Wen et al., 2023). Vehicular NH_3 emissions are known to contribute to the rapid formation of fine particulate matter, particularly during air pollution episodes, underscoring the predominant role of fossil fuel combustion as a non-agricultural NH_3 source in urban environments (Farren et al., 2020, 2021; Pan et al., 2016). Additionally, various industrial activities including steel production (Chen and Wang, 2025), power generation, and fertilizer manufacturing also release substantial amounts of NH_3 into the atmosphere (Van Damme et al., 2018; Gu et al., 2023).~~

L98: The authors seem to use the words “emission” and “concentration” interchangeably throughout the paper, including here where it says the authors will first detail the spatiotemporal variability of NH3 emissions. Another example is Figures 2 and 3, which captions both say “NH3 emissions (molecules/cm^2)”, but these are the units of column concentrations (or more precisely, total columns), not emissions. “Emission” and “concentration” have different scientific meanings and should not be mixed, as deriving emissions from column concentrations requires more than satellite observations and typically involves a modeling approach.

We thank the reviewer for pointing out this inconsistency. In the revised manuscript, we have removed all the references of emission and concentration, now consistently refer only to NH_3 total column (molecules cm^{-2}), this includes text, figures, tables, and supplementary document, unless explicitly referring to values reported in external literature.

L172: This detection limit (4–6×10^15 molecules/cm^2) was for an earlier version of IASI product. Is there an updated number for version 4? As mentioned earlier, this becomes relevant because the reported annual mean NH3 concentrations over Guatemala (4.12–6.67×10^15 molecules/cm^2) are very close to the detection limit of IASI. Can we realistically draw conclusions on the interannual trends when the mean concentrations are so low? Would other satellite instruments that have higher sensitivities to surface NH3 be better options?

We Thank the reviewer for this comment, and we acknowledge the concern regarding the detection limit. The detection limit (4–6×10^15 molecules/cm^2) referenced for previous studies and retrieval version. The current version is v4.0.1R (2024/10/25 – current). For our study (2015–2023) we used ANNI-NH_3 v4.0.0R ULB-LATMOS L3 gridded average (spatial and temporal) (available version 2023/07/03 – 2024/10/25) that reduces random error and improve the effective sensitivity. Version 4 incorporates retrieval improvements, updated spectroscopy, enhanced uncertainty characterization, and improved column values that are about 15–20% larger due the upgraded Hyperspectral Range Index (HRI) (Clarisse et al., 2023).

The detection capability cannot be described by a single threshold, because the retrieval sensitivity depends on several factors including thermal contrast, cloud fraction, and surface condition (Clarisse et al., 2023; Van Damme et al., 2017). Thus, to avoid potential confusion, the detection limit of IASI cited in the old version has been removed from the manuscript. The robustness of the results is supported by a relative high data volume with an average of 1,395 pixels per month, with the standard error annual means remains lower (1.65×10^{14} molecules cm^{-2} to 1.68×10^{15} molecules cm^{-2}) (Table S9, S10). Additionally, Guatemala is situated in a tropical region where the thermal contrast is generally favorable for thermal contrast (latitude 13.5°–17.8° N). Contrary to relatively colder areas, such higher latitudes are linked to limited thermal contrast, which limits the sensitivity of nadir sounders to surface concentrations (Clarisse et al., 2009; Franco et al., 2018).

Regarding to draw conclusions on the interannual trends when the mean concentrations are so low? To assess if the interannual variability can be robustly enough to be interpreted, we compared the magnitude of the variability with the relative uncertainty, as we mentioned above then we computed a correlation analysis of concatenated NH_3 columns and monthly observation density (Fig. S9). The minor correlation R^2 =0.028 and p=0.082, suggest that the variability in total columns is large enough and independent of how often the sensors observe the area of Guatemala. Specifically for the year 2020 (1.97 obs. grid cell month per month) where was the highest mean total column of NH_3, this value is 17% relative lower respecting the previous year for the observation density, likely due to increase on cloud cover, however it reminded sufficiently to obtain the maximum of NH_3.

Regarding the use of other satellite sensors to detect higher sensitive to surface NH_3, IASI provides different sensors with a consistency and stable spatio-temporal resolution, that is suitable for interannual variability. For this reason, we focused on IASI for homogeneity across Guatemala.

Table S9: Annual summary of statistics of the of the concatenated NH_3 total column density, and IASI metrics over Guatemala (2015–2023). The table include annual mean (molecules cm^{-2}), standard error of the mean (SEM) (molecules cm^{-2}), relative uncertainty (%), total pixel counts, and mean monthly observations per 0.25 grid cell.

Year	Annual Mean (molec cm^{-2})	Standard Error (molec cm^{-2})	Relative Uncertainty (%)	Total Pixel (annual sum)	Obs. Grid Cell $Month^{-1}$
2015	4.64×10^{15}	4.58×10^{14}	9.85	15696	2.16
2016	6.27×10^{15}	1.52×10^{15}	24.26	15931	2.19
2017	4.43×10^{15}	2.78×10^{14}	6.27	17142	2.36
2018	4.08×10^{15}	2.25×10^{14}	5.52	18286	2.52
2019	5.12×10^{15}	7.38×10^{14}	14.43	19255	2.65
2020	6.68×10^{15}	1.68×10^{15}	25.19	14305	1.97
2021	3.99×10^{15}	1.65×10^{14}	4.14	15162	2.09
2022	4.41×10^{15}	2.94×10^{14}	6.68	13432	1.85
2023	5.48×10^{15}	8.09×10^{14}	14.76	16485	2.27

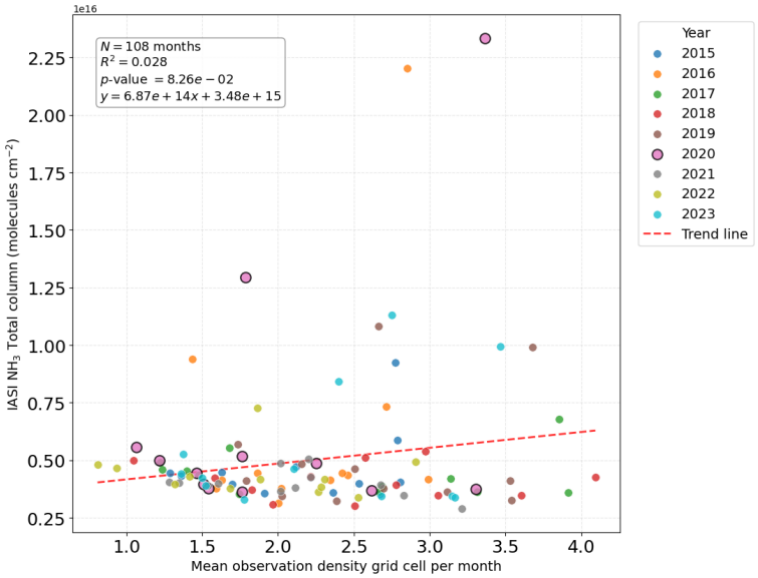

Figure S9: Correlation analysis of the concatenated monthly NH_3 total column and observation per grid cell per month over Guatemala (2015–2023), each point represents the monthly average with a specific colour by year. The weak correlation (R^2=0.028

and p<0.001) suggest the annual variability of NH_3 that is large independent of sample frequency. The 2020 (black edge circle) demonstrate highest column (April, top-right) despite the moderate observation sample density.

Figure 2: How much do the measurements vary between the three IASI instruments? Can you show some statistics of NH3 columns by instrument? Without knowing this, this figure feels like comparing apples to oranges because not all years are covered by the same IASI instruments.

It would also be interesting to see if the number of IASI pixels are significantly different 1) between the years, and 2) between the low concentration grids and high concentration grids. This helps to understand whether the low concentrations are affected by sampling bias. Can you also describe how the IASI algorithm handles spatial averaging/weighting in the L3 data?

We thank the reviewer for this comment. To ensure continuity across IASI instruments, we conducted a comparison using IASI-B (January 2015–December 2023) as the reference sensor because covers the long-term period analysis compared with A (January 2015–December 2020), and C (January 2020–December 2023). During overlapping observation periods, the sensors exhibited strong agreement. The comparison between IASI-A and IASI-B, based on 72 overlapping months, yielded a coefficient of determination (R^2) of 0.93. In comparison, IASI-C and IASI-B, with 48 overlapping months, demonstrated a stronger relationship with $R^2 = 0.98$. Linear regression slopes were 0.96 (IASI-A and IASI-B), and 0.99 (IASI-C and IASI-B), neither was statistically different from 1 ($p > 0.05$), indicating strong agreement between the instruments.
A paired t-test revealed no statistically significant mean difference between IASI-A and IASI-B ($p = 0.18$), while IASI-C and IASI-B was statistically significant ($p < 0.01$). However, the magnitude of this difference was small, with mean biases of -1.46×10^{14} molecules cm^{-2} for IASI-A versus IASI-B and 2.45×10^{14} molecules cm^{-2} for IASI-C versus IASI-B. These values are minor compared to the long term mean total column over Guatemala (5.01×10^{15} molecules cm^{-2}) and with the standard error (1.65×10^{14} molecules cm^{-2} to 1.68×10^{15} molecules cm^{-2}), (Table S9). The corresponding to relative differences of approximately 2–5% of the mean column are smaller than the observed annual and climatology variability, therefore the concatenated dataset is suitable for our study with long term column analysis over Guatemala.

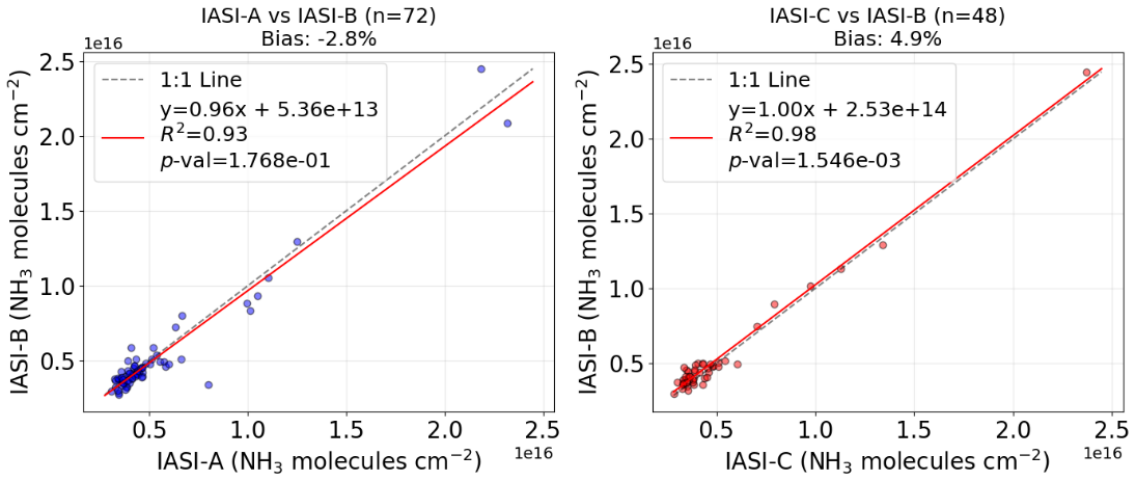

Figure S8: Scatter plots monthly mean comparison of IASI A/B/C sensors. (Left), IASI A-B for 73 overlapping months. (Right), IASI C-B for 48 overlapping months.

For the observation sampling bias, the annual mean sampling density remained robust through the study period (1.85–2.65 obs. grid cell month per month). Specifically for the year 2020 (1.97 obs. grid cell month per month) where was the highest mean total column of NH_3, this value is 17% relative lower respecting the previous year for the observation density, likely due to increase on cloud cover, however it reminded sufficiently to obtain the maximum of NH_3.

Regarding the relationship between observation and total column, the Fig. S9, shows a linear regression between monthly total columns of NH_3 and observations density across the 108 months. It demonstrates no significant correlation R_2=0.028 and no significance with p=0.082.

The spatial area-wide mean observation grid cell ranged from 0.68–3.68 obs. grid cell month per month. The lowest observation occurs over high altitude terrain (~2700 m a.s.l.), located in the Sierra de las Minas, Alta Verapaz department (approx. 15.19°N, 89.69°W). In these areas, persistent cloud cover associated with the tropical cloud forest that is characterized by high annual precipitation (600–2500 mm yr^{-1}), elevated relative humidity (67%–95%), and lower surface temperatures (5° to 25°C) (Chaluleu, 2020; Holder, 2003, 2006). This extreme condition frequently limits infrared retrievals.

Finally, the L3 algorithm utilizes arithmetic averaging of 0.25° x 0.25° grid cell presented in level 2 (L2) pixel centres falling withing that cell. Thus, no extra spatial interpolation or distance based weighted were applied, to ensure that L3 dataset remains of its original IASI measurement. By concatenating IASI A, B and C, we used a total of 228 observations of sensor months over the 108 months of the study period increasing the signal to noise ratio and spatial representativeness.

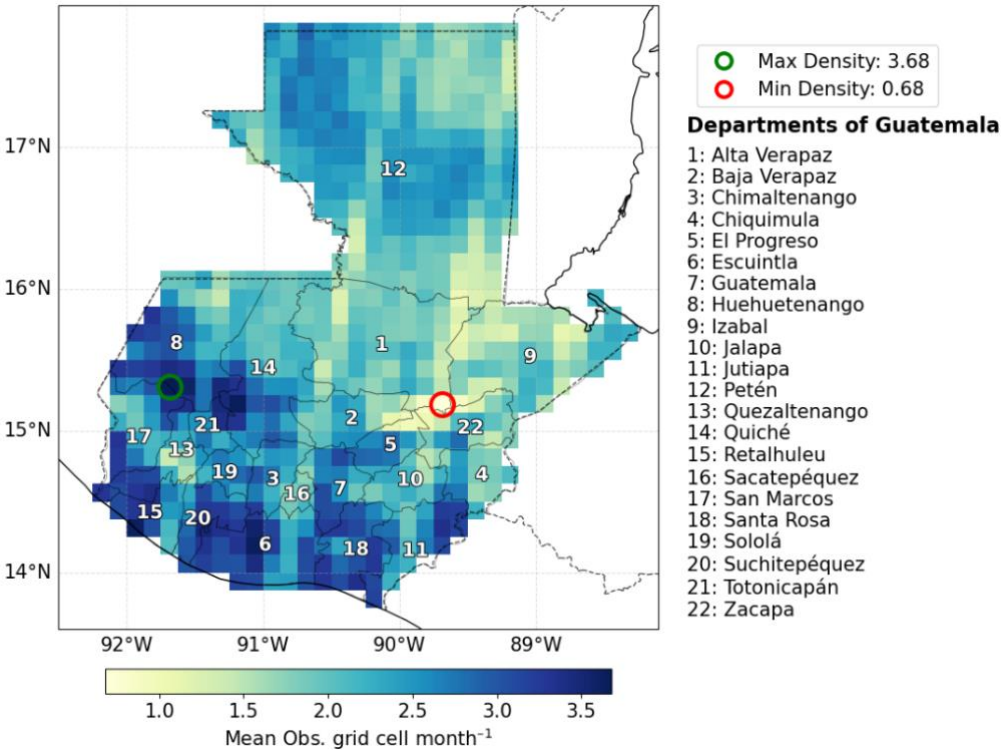

Figure S10: Spatial area-wide of means of observation grid cell month per month over Guatemala (2015–2023), representing the highest and lowest distribution detection, green circle showing the highest and with the red circle showing the lowest density obs. located in Sierra de las Minas, Alta Verapaz department (15.19°N, 89.69°W).

Table S10: Annual summary of statistics of the observation density grid cell per month and pixel per month over Guatemala (2015–2023)

Observation density grid cell per month

Year	Annual Mean	Standard deviation	Min	Median	Max
2015	2.16	0.57	1.29	2.24	2.81
2016	2.19	0.52	1.44	2.18	2.99
2017	2.36	1.02	1.22	2.21	3.91
2018	2.52	0.86	1.04	2.54	4.09
2019	2.65	0.68	1.74	2.59	3.68
2020	1.97	0.76	1.07	1.76	3.37
2021	2.09	0.60	1.28	2.07	3.21
2022	1.85	0.64	0.81	1.87	2.91
2023	2.27	0.77	1.36	2.25	3.47

Pixel per month

Year	Annual Mean	Standard deviation	Min	Median	Max
2015	1177	401	575	1137	1679
2016	1222	375	785	1155	1797
2017	1316	663	574	1205	2332
2018	1391	571	485	1421	2464
2019	1492	479	755	1423	2223
2020	1145	488	573	991	2037
2021	1140	389	598	1112	1868
2022	978	428	300	1036	1741
2023	1249	521	669	1297	2097

L407: "…which points to a general inverse relationship where higher NH3 concentrations tend to coincide with lower PBLH values, and vice versa. This pattern suggests that a shallower boundary layer, which restricts the vertical dispersion, leads to an accumulation of NH3 near the surface." This explanation would hold true for surface NH3 concentrations. However, IASI measures vertically integrated columns which are less sensitive to fluctuations in BLH. Figure 7 also does not quite reflect an inverse relationship between IASI and BLH. In fact, the Pearson correlation matrix in Figure S3 even shows NH3 and BLH are moderately positively correlated.

We thank the reviewer for pointing this out. In the old version, the description related of the NH_3 and BHL was imprecise and could lead to confusion. In the revised manuscript, Fig. 7, we use a boxplot distribution of meteorological variable rather than combining them with NH_3 timeseries. Now the analysis focuses on the statistical variability of BLH, temperature, relative humidity, and precipitation. Additionally, the quantitative relationship of NH_3 and meteorological variables in the Pearson correlation is described in the discussion section. Also, the old version Fig. 7 timeseries has been moved to supplementary document (Fig. S4).

REVISED MANUSCRIPT (L346-L365)

Figure 7 illustrates the variability of meteorological variables derived from monthly scales over Guatemala from ERA5. Fig. 7 (a,c), exhibit the BLH and precipitation. The BLH shows fluctuations with the highest median recorded in 2019 (524 m), in contrast to the lowest median observed in 2017 (415 m) which also demonstrated the minimum value (305 m) (Table S6). The maximum vertical value was detected during 2020 (791 m) indicated a large data range. At the monthly scale, April shows the highest BLH (median 671 m) and lowest during October (median 348 m). Furthermore, the precipitation indicates that the annual distribution of monthly totals presents the highest median values recorded in 2020 (69 mm) and 2022 (55 mm), while the lowest median is observed in 2019 (34 mm) which also shows the minimum value (7.5 mm). The maximum monthly exceeds

130 mm (2017 and 2022). The monthly climatology presents peaks medians precipitation in the month of June (97 mm), and September (95 mm), while the lowest in February (13 mm).

Fig. 7(b,e) present the air temperature and relative humidity. The warmest median temperature during the year 2023 (22.8°C), whereas the maximum temperature was detected during 2020 (27.9°C). The coldest temperature was recorded during 2018 with 20.2°C. Additional, the warmest month is May (median 26.4°C) and the coldest is January (21.9°C). Relative humidity showed the highest median observed during 2016 (81%), while the lowest median year was 2019 (76%), the minimum year detected was 2020 with 63%, this also showed the largest vertical values. The years 2017 and 2022 exhibit the maximum values with 87%. The month medians indicate the lowest in April (mean 71%) and the highest in October (mean 84%).

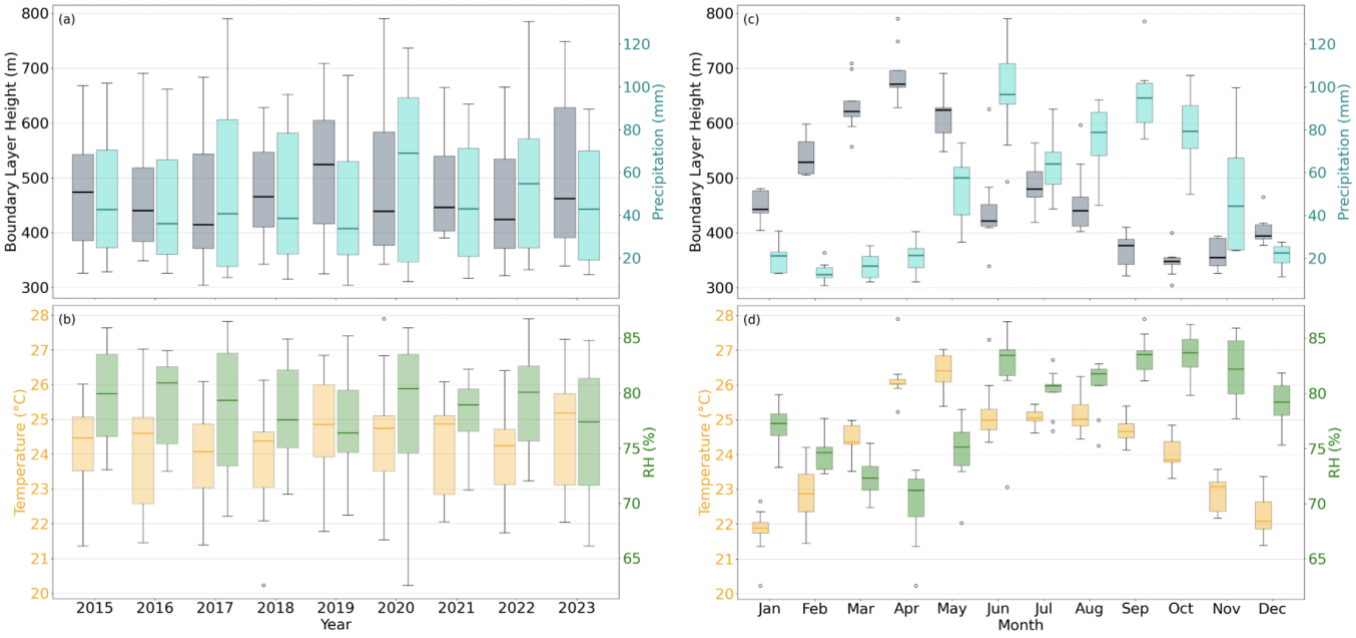

Figure 7: Boxplot distribution of meteorological variables over Guatemala (2015–2023) from ERA5 reanalysis, (a, c) show boundary layer height (m) (gray) and precipitation (mm) (turquoise), (b, d) relative humidity (%) (green) and temperature (°C) (yellow).

L565: Sometimes I find it difficult to associate the argument with the results supporting it. For example, here it says the high number of fires in April 2020 was likely driven by prolonged dry conditions. This initially confused me because the following sentence says the year 2020 recorded the highest total precipitation. I had to look through the paper again to see that April 2020 indeed had one of the lowest monthly precipitations according to Figure 7, but this was never explicitly called out.

We thank the reviewer for this important comment regarding more clarity of fires and atmospheric conditions during April 2020, which might lead to confusion. While 2020 showed of the highest annual total precipitation (707 mm) (Table S6), the

dataset also shows relatively low minimum month precipitations (9 mm) following 2019 (7.5 mm), indicating the occurrence of the shortly dry period within that year. This year coincide with peak fire activity, highest temperature recorded (27.9° C) and highest BHL (791 m), created favourable conditions of fire increase and observed NH_3 peak (Fig. S4) (L446–465).

Finally, a lot of interesting results presented in Figure S3 were never discussed in the main text. In particular, it was mentioned in section 2.1 that the interrelationships between NH3 and other air pollutants (NO2 and SO2) will be explored, but they were not. Also, what are the sources of the NO2 and SO2 data (satellite observations or surface measurements)?

We thank the reviewer for this comment. In the revised manuscript we wanted to keep the consistency of NH_3 and variables not direct discussed were removed from the analysis (surface pressure (sp), Nitrate Dioxide (NO_2) and Sulphur Dioxide (SO_2)). In the old version the NO_2 and SO_2 were retrieved from global reanalysis CAMS.

Minor comments:

L81: When you say "previous research has often overlooked the integrated role of multiple environmental drivers…" without giving examples, it is unclear to me which studies you are referring to, since you also mention there is a significant lack of studies on Central America. Can you add some references?

Thank you for the suggestion. In the revised manuscript, for the Introduction section, we have revised and clarified the paragraph, regarding the limited integration of multiple variables to assess the integrated analysis combining NH_3, fires, meteorology, and land cover.

REVISED MANUSCRIPT (L71-L77)

Despite the increasing availability of satellite-based datasets for monitoring atmospheric NH_3, there remains a significant lack of regional-scale studies in Central America, particularly in Guatemala, where land use dynamics and biomass burning are likely to play an important role in shaping substantially to atmospheric NH_3 patterns. Previous research has primarily examined individual drivers, such as meteorological circulation and fire season in Central America (Corona-Núñez and Campo, 2023; Liu et al., 2024), or continental scale assessment of NH_3 variability (Clarisse et al., 2009; Van Damme et al., 2021; Herrera et al., 2022; Luo et al., 2022; Zhu et al., 2015). However, integrated regional analysis that simultaneously consider concatenated NH_3, fire activity, land cover and meteorological variables remain limited.

L174: The authors may also want to double check the existing citations. For example, the 2012 paper cited here seems unrelated to IASI.

We thank the reviewer for the comment. In the revised manuscript we have made the corrections regarding the correct citation for IASI (L119).

L195: This equation does not look right. It is missing an equal sign, and the square root sign should extend further. Please double check this equation and also Equation (2).

We thank the reviewer for raising this point, in the revised manuscript we have made the corrections for equitation (1) (L161) and (2) (L167).

L240: This should be Equation (3).

In the revised manuscript we have made the corrections and add the Equation (3) (L219).

L314: "3.2 Land cover classification driven a k-means clustering of NH3 emissions" This subtitle needs some grammar editing.

We thank the reviewer for the comment. In the revised manuscript we changed the subtitle (3.2 Land cover classification driven by NH_3 cluster k-means) (~~Land cover classification driven a k-means clustering of NH_3 emissions~~), (L274).

L341: Here it says Cluster 1 covers the smallest area compared to Cluster 2 and Cluster 3. However, the paragraph above says Cluster 3 has the smallest territorial extent. I do not understand the difference.

We thank the reviewer for this comment. In the old version, the contradictory text was made regarding the extent area of cluster 1 and 3. In the revised manuscript we modified the area supported by Table 1, and cluster 1 present the smallest area extent (~28,254 km^2), cluster 2 with larger area extent (~45,662 km^2) and cluster 3 with intermediate (~34,640 km^2), (L280-L297).

L355: Why does it suddenly say ammonium (NH4+) here?

We thank the reviewer for this comment. In the revised manuscript we change to specify NH_3 and not ammonium (L309).

L453: ppmv does not need to be in uppercase. Also, instead of writing 1.55 × 10^–3 ppmv, it is more natural to say 1.55 ppbv.

We thank the reviewer for the suggestion. In the old version NH_3 mixing ratios were expressed in ppmv and total column units. In the revised manuscript the sentence has been corrected to consistently report CAMS reanalysis in mass mixing ratios kg kg^{-1}. The ppmv notation has been removed and no conversion to column unit is applied in this section to ensure the dimensional

consistency. Therefore, we use to illustrate the NH_3 structure in (kg kg^{-1}), rather than for quantitative comparison with IASI total column (Results, L381-L396). Additionally, we explain in the methodology section the description regarding the vertical and latitudinal profiles from CAMS mass mixing ratios (Methodology, L140-L148).

REVISED MANUSCRIPT (Methodology, L140-L148)

Additionally, NH_3 vertical profiles data were obtained from the ECMWF, Atmospheric Composition Reanalysis 4 (EAC4), produced by CAMS. This reanalysis provides NH_3 with mass fraction in the air, provided as a mass mixing ratio (kg kg^{-1}), the model is defined by 60 hybrid sigma-pressure levels. It provides a detailed representation of the atmospheric structure, particularly near the surface (~0–100 m) where most emissions occur (Inness et al., 2019). These reanalysis datasets incorporate satellite observations and model simulations to provide globally consistent, spatially and temporally resolved atmospheric composition data (Flemming et al., 2017; Inness et al., 2019). In this study, the CAMS analysis of vertical structure and latitudinal distribution of NH_3 during a specific period of interest, rather than for a quantitative comparison with satellite of total column densities.

REVISED MANUSCRIPT (Results, L381-L396)

Figure 9a shows the vertical and latitudinal distribution of atmospheric NH_3 over Guatemala using zonal means and area averaged vertical profiles in mass mixing ratios (kg kg^{-1}). The zonal mean cross-section of NH_3 throughout the atmosphere (vertical axis, model level 60 to 44) along the latitudes of Guatemala as a zonal mean during April 2020. It highlights a greater abundance of NH_3 in both the northern and southern areas. Furthermore, the NH_3 vary with both latitude and altitude, the highest NH_3 are observed at lower model levels primarily confined near the surface (below approximately level 56). The highest NH_3 values are found between 14°N and 15°N latitude.

Fig. 9b further illustrates the area average vertical profiles of NH_3 for April (blue line), spring (March – May, green line) and the annual mean 2020 (black dashed line). The vertical profile of NH_3 shows the April 2020 mean (blue line) with ~1.0×10^{-9} kg kg^{-1}, the spring mean (March–May 2020, green line) of ~0.9×10^{-9} kg kg^{-1} and the annual mean for 2020 (black dashed line) with ~0.5×10^{-9} kg kg^{-1} respectively.

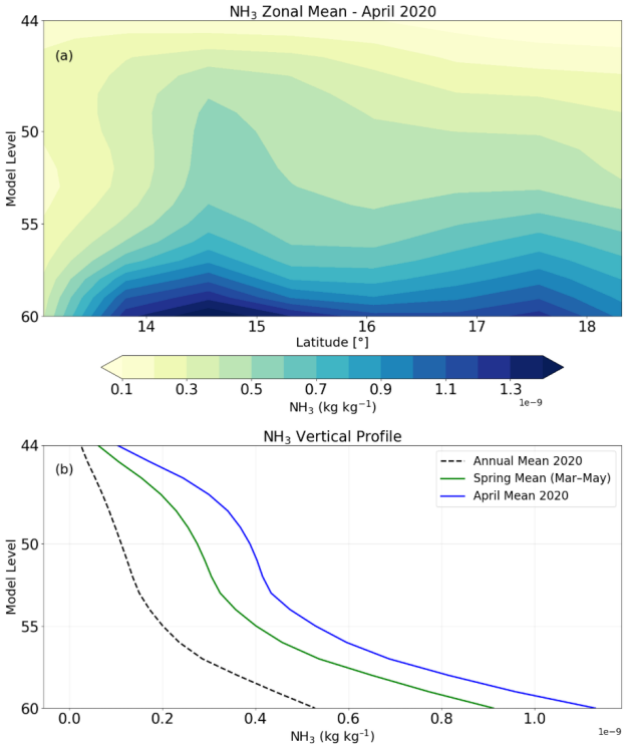

Figure 9: (a) zonal mean of NH_3 mass mix ratio (kg kg^{-1}) ~~total column (× 10^{16} molecules cm^{-2})~~ across latitudinal bands (model level 60 to 44) for April 2020 and (b) vertical profile of NH_3 mass mix ratio (kg kg^{-1}) for April (blue line), spring (March – May, green line) and annual mean 2020 (black dashed line) over Guatemala from global reanalysis CAMS.

References

Abeed, R., Viatte, C., Porter, W. C., Evangeliou, N., Clerbaux, C., Clarisse, L., Van Damme, M., Coheur, P.-F., and Safieddine, S.: Estimating agricultural ammonia volatilization over Europe using satellite observations and simulation data, EGUsphere, https://doi.org/10.5194/egusphere-2022-1046, 2022.

Chaluleu, C. A.: Fototrampeo en bosques nubosos y latifoliados de la Reserva de la Biósfera Sierra de las Minas, Revista Mesoamericana de Biodiversidad y Cambio Climático–Yu'am, 4, 44–65, 2020.

Chen, P. and Wang, Q.: Underestimated industrial ammonia emission in China uncovered by material flow analysis, Environmental Pollution, 368, 125740, https://doi.org/10.1016/j.envpol.2025.125740, 2025.

Chen, P., Wang, Q., Shao, M., and Liu, R.: Significantly underestimated traffic-related ammonia emissions in Chinese megacities: Evidence from satellite observations during COVID-19 lockdowns, Chemosphere, 361, 142497, https://doi.org/10.1016/j.chemosphere.2024.142497, 2024.

Clarisse, L., Clerbaux, C., Dentener, F., Hurtmans, D., and Coheur, P.-F.: Global ammonia distribution derived from infrared satellite observations, Nat. Geosci., 2, 479–483, https://doi.org/10.1038/ngeo551, 2009.

Clarisse, L., Franco, B., Van Damme, M., Gioacchino, T. Di, Hadji-Lazaro, J., Whitburn, S., Noppen, L., Hurtmans, D., Clerbaux, C., and Coheur, P.: The IASI NH 3 version 4 product: averaging kernels and improved consistency, Atmos. Meas. Tech., 16, 5009–5028, https://doi.org/10.5194/amt-2023-48, 2023.

Corona-Núñez, R. O. and Campo, J. E.: Climate and socioeconomic drivers of biomass burning and carbon emissions from fires in tropical dry forests: A Pantropical analysis, Glob. Chang. Biol., 29, 1062–1079, https://doi.org/10.1111/gcb.16516, 2023.

Van Damme, M., Whitburn, S., Clarisse, L., Clerbaux, C., Hurtmans, D., and Coheur, P.-F.: Version 2 of the IASI NH3 neural network retrieval algorithm: near-real-time and reanalysed datasets, Atmos. Meas. Tech., 10, 4905–4914, https://doi.org/10.5194/amt-10-4905-2017, 2017.

Van Damme, M., Clarisse, L., Whitburn, S., Hadji-Lazaro, J., Hurtmans, D., Clerbaux, C., and Coheur, P.-F.: Industrial and agricultural ammonia point sources exposed, Nature, 564, 99–103, https://doi.org/10.1038/s41586-018-0747-1, 2018.

Van Damme, M., Clarisse, L., Franco, B., Sutton, M. A., Erisman, J. W., Wichink Kruit, R., van Zanten, M., Whitburn, S., Hadji-Lazaro, J., Hurtmans, D., Clerbaux, C., and Coheur, P.-F.: Global, regional and national trends of atmospheric ammonia derived from a decadal (2008–2018) satellite record, Environmental Research Letters, 16, 055017, https://doi.org/10.1088/1748-9326/abd5e0, 2021.

Dragosits, U., Theobald, M. R., Place, C. J., Lord, E., Webb, J., Hill, J., ApSimon, H. M., and Sutton, M. A.: Ammonia emission, deposition and impact assessment at the field scale: a case study of sub-grid spatial variability, Environmental Pollution, 117, 147–158, https://doi.org/10.1016/S0269-7491(01)00147-6, 2002.

Farren, N. J., Davison, J., Rose, R. A., Wagner, R. L., and Carslaw, D. C.: Underestimated Ammonia Emissions from Road Vehicles, Environ. Sci. Technol., 54, 15689–15697, https://doi.org/10.1021/acs.est.0c05839, 2020.

Farren, N. J., Davison, J., Rose, R. A., Wagner, R. L., and Carslaw, D. C.: Characterisation of ammonia emissions from gasoline and gasoline hybrid passenger cars, Atmos. Environ. X, 11, 100117, https://doi.org/10.1016/j.aeaoa.2021.100117, 2021.

Flemming, J., Benedetti, A., Inness, A., Engelen, R. J., Jones, L., Huijnen, V., Remy, S., Parrington, M., Suttie, M., Bozzo, A., Peuch, V.-H., Akritidis, D., and Katragkou, E.: The CAMS interim Reanalysis of Carbon Monoxide, Ozone and Aerosol for 2003–2015, Atmos. Chem. Phys., 17, 1945–1983, https://doi.org/10.5194/acp-17-1945-2017, 2017.

Franco, B., Clarisse, L., Stavrakou, T., Müller, J. -F, Van Damme, M., Whitburn, S., Hadji-Lazaro, J., Hurtmans, D., Taraborrelli, D., Clerbaux, C., and Coheur, P. -F: A General Framework for Global Retrievals of Trace Gases From IASI: Application to Methanol, Formic Acid, and PAN, Journal of Geophysical Research: Atmospheres, 123, https://doi.org/10.1029/2018JD029633, 2018.

Gu, C., Wang, S., Zhu, J., Dai, W., Liu, J., Xue, R., Che, X., Lin, Y., Duan, Y., Wenig, M. O., and Zhou, B.: Underestimated ammonia vehicular emissions in metropolitan city revealed by on-road mobile measurement, Environmental Research Letters, 18, 104040, https://doi.org/10.1088/1748-9326/acf94a, 2023.

Herrera, B., Bezanilla, A., Blumenstock, T., Dammers, E., Hase, F., Clarisse, L., Magaldi, A., Rivera, C., Stremme, W., Strong, K., Viatte, C., Van Damme, M., and Grutter, M.: Measurement report: Evolution and distribution of NH3 over Mexico City from ground-based and satellite infrared spectroscopic measurements, Atmos. Chem. Phys., 22, 14119–14132, https://doi.org/10.5194/acp-22-14119-2022, 2022.

Holder, C. D.: Fog precipitation in the Sierra de las Minas Biosphere Reserve, Guatemala, Hydrol. Process., 17, 2001–2010, https://doi.org/10.1002/hyp.1224, 2003.

Holder, C. D.: The hydrological significance of cloud forests in the Sierra de las Minas Biosphere Reserve, Guatemala, Geoforum, 37, 82–93, https://doi.org/10.1016/j.geoforum.2004.06.008, 2006.

Inness, A., Ades, M., Agustí-Panareda, A., Barré, J., Benedictow, A., Blechschmidt, A.-M., Dominguez, J. J., Engelen, R., Eskes, H., Flemming, J., Huijnen, V., Jones, L., Kipling, Z., Massart, S., Parrington, M., Peuch, V.-H., Razinger, M., Remy, S., Schulz, M., and Suttie, M.: The CAMS reanalysis of atmospheric composition, Atmos. Chem. Phys., 19, 3515–3556, https://doi.org/10.5194/acp-19-3515-2019, 2019.

Liu, Y., Qian, Y., Rasch, P. J., Zhang, K., Leung, L. R., Wang, Y., Wang, M., Wang, H., Huang, X., and Yang, X.-Q.: Fire–precipitation interactions amplify the quasi-biennial variability in fires over southern Mexico and Central America, Atmos. Chem. Phys., 24, 3115–3128, https://doi.org/10.5194/acp-24-3115-2024, 2024.

Luo, Z., Zhang, Y., Chen, W., Van Damme, M., Coheur, P.-F., and Clarisse, L.: Estimating global ammonia (NH_3) emissions based on IASI observations from 2008 to 2018, Atmos. Chem. Phys., 22, 10375–10388, https://doi.org/10.5194/acp-22-10375-2022, 2022.

Pan, Y., Tian, S., Liu, D., Fang, Y., Zhu, X., Zhang, Q., Zheng, B., Michalski, G., and Wang, Y.: Fossil Fuel Combustion-Related Emissions Dominate Atmospheric Ammonia Sources during Severe Haze Episodes: Evidence from ^{15}N-Stable Isotope in Size-Resolved Aerosol Ammonium, Environ. Sci. Technol., 50, 8049–8056, https://doi.org/10.1021/acs.est.6b00634, 2016.

Sun, K., Tao, L., Miller, D. J., Pan, D., Golston, L. M., Zondlo, M. A., Griffin, R. J., Wallace, H. W., Leong, Y. J., Yang, M. M., Zhang, Y., Mauzerall, D. L., and Zhu, T.: Vehicle Emissions as an Important Urban Ammonia Source in the United States and China, Environ. Sci. Technol., 51, 2472–2481, https://doi.org/10.1021/acs.est.6b02805, 2017.

Sutton, M. A., Nemitz, E., Erisman, J. W., Beier, C., Bahl, K. B., Cellier, P., de Vries, W., Cotrufo, F., Skiba, U., Di Marco, C., Jones, S., Laville, P., Soussana, J. F., Loubet, B., Twigg, M., Famulari, D., Whitehead, J., Gallagher, M. W., Neftel, A., Flechard, C. R., Herrmann, B., Calanca, P. L., Schjoerring, J. K., Daemmgen, U., Horvath, L., Tang, Y. S., Emmett, B. A., Tietema, A., Peñuelas, J., Kesik, M., Brueggemann, N., Pilegaard, K., Vesala, T., Campbell, C. L., Olesen, J. E., Dragosits, U., Theobald, M. R., Levy, P., Mobbs, D. C., Milne, R., Viovy, N., Vuichard, N., Smith, J. U., Smith, P., Bergamaschi, P., Fowler, D., and Reis, S.: Challenges in quantifying biosphere–atmosphere exchange of nitrogen species, Environmental Pollution, 150, 125–139, https://doi.org/10.1016/j.envpol.2007.04.014, 2007.

Wen, Y., Zhang, S., Wu, Y., and Hao, J.: Vehicular ammonia emissions: an underappreciated emission source in densely populated areas, Atmos. Chem. Phys., 23, 3819–3828, https://doi.org/10.5194/acp-23-3819-2023, 2023.

Wyer, K. E., Kelleghan, D. B., Blanes-Vidal, V., Schauberger, G., and Curran, T. P.: Ammonia emissions from agriculture and their contribution to fine particulate matter: A review of implications for human health, J. Environ. Manage., 323, 116285, https://doi.org/10.1016/j.jenvman.2022.116285, 2022.

Zhou, Y., Zhao, Y., Mao, P., Zhang, Q., Zhang, J., Qiu, L., and Yang, Y.: Development of a high-resolution emission inventory and its evaluation and application through air quality modeling for Jiangsu Province, China, Atmos. Chem. Phys., 17, 211–233, 2017.

Zhu, L., Henze, D. K., Bash, J. O., Cady-Pereira, K. E., Shephard, M. W., Luo, M., and Capps, S. L.: Sources and Impacts of Atmospheric NH3: Current Understanding and Frontiers for Modeling, Measurements, and Remote Sensing in North America, Curr. Pollut. Rep., 1, 95–116, https://doi.org/10.1007/s40726-015-0010-4, 2015.